

RSC Advances



This is an *Accepted Manuscript*, which has been through the Royal Society of Chemistry peer review process and has been accepted for publication.

Accepted Manuscripts are published online shortly after acceptance, before technical editing, formatting and proof reading. Using this free service, authors can make their results available to the community, in citable form, before we publish the edited article. This *Accepted Manuscript* will be replaced by the edited, formatted and paginated article as soon as this is available.

You can find more information about *Accepted Manuscripts* in the [Information for Authors](#).

Please note that technical editing may introduce minor changes to the text and/or graphics, which may alter content. The journal's standard [Terms & Conditions](#) and the [Ethical guidelines](#) still apply. In no event shall the Royal Society of Chemistry be held responsible for any errors or omissions in this *Accepted Manuscript* or any consequences arising from the use of any information it contains.

Structural characterization of metal dopants (M = Ag or Au) in
trimetallic M–Pd–Pt clusters

Xia Wu^{1*}, Qiman Liu¹, Yan Sun², Genhua Wu¹

¹ *School of Chemistry and Chemical Engineering, Anqing Normal University,
Anqing 246011, PR China*

² *College of Chemical Engineering, Hebei United University, Tangshan 063009, PR
China*

Corresponding address:

School of Chemistry and Chemical Engineering,
Anqing Normal University, Anqing, 246011, P. R. China.

Tel: +86-556-550-0090

Fax: +86-556-550-0090

E-mail: xiawu@aqtc.edu.cn

* Corresponding author.

Abstract

The structures and properties of bimetallic Pd–Pt clusters are affected by altering metal dopants in trimetallic M–Pd–Pt (M = Ag and Au) clusters. The M–Pd–Pt clusters with up to 75 atoms are studied to investigate the structural difference caused by metal dopants, which are optimized by adaptive immune optimization algorithm (AIOA). The tight-binding Gupta potential is adopted to describe the interatomic interactions in the trimetallic clusters. Results show that there exist significant difference between the stable structures of Ag–Pd–Pt and Au–Pd–Pt clusters for the investigated clusters. The dominant motif of 13-atom clusters is Mackay icosahedron except for some non-icosahedral configurations, and the number of non-icosahedra in Au–Pd–Pt clusters is larger than that in Ag–Pd–Pt clusters. Furthermore, there exist many mixed decahedron/close-packed motifs in both clusters as in Pd–Pt clusters. It is also the dominant motif of 75-atom Ag–Pd–Pt clusters, however, in Au–Pd–Pt clusters corresponding motif is Marks decahedron. Moreover, the atomic distribution of Pd and Pt atoms in Ag–Pd–Pt clusters is similar to that in Au–Pd–Pt clusters, but Au atoms grow more closely than Ag atoms. On the other hand, the relative stability for both clusters is compared by the second order finite difference parameter.

Keywords: trimetallic clusters; global optimization; immune optimization algorithm; Gupta potential; structural stability

1. Introduction

Nanoscale materials such as alloyed multimetallic clusters have been widely studied because of great importance for their diverse range of electrical, optical and catalytic properties.¹⁻³ Bimetallic clusters often exhibited enhanced catalytic reaction performance compared to the pure metals due to wide selectivity and stability.^{4,5} Trimetallic clusters are an active research field,⁶ and in many cases their catalytic activity is superior to bimetallic clusters.^{7,8} For instance, the activity of the Au/Pt/Ag trimetallic nanoparticles was several times higher than that of Au nanoparticles with nearly the same particle size.⁷ Pt–Ru–Co metallic nanoparticles could enhance catalytic activity towards methanol oxidation compared to Pt–Ru bimetallic nanoparticles.⁸ Moreover, Au–Pd–Pt trimetallic clusters showed superior oxygen reduction reaction electrocatalytic activity compared with the Pd–Pt and Au–Pt bimetallic clusters.⁹ In theoretical studies, Monte Carlo and molecular dynamics simulations were used to investigate the effect of composition and size on the structures and melting behavior of icosahedral Au–Pd–Pt trimetallic clusters with different compositions and sizes.¹⁰

Bimetallic Pd–Pt catalyst represents an important system in catalysis research, which exhibits high activities in the hydrogenation of aromatics.¹¹ Computational studies based on the Gupta many-body potential have given the stable geometrical structures of Pd–Pt clusters with 34, 38, and 98 atoms.^{12,13} Results showed that decahedral motifs dominated for 34-atom Pd–Pt clusters, and segregation effects of Pd atoms to the surface of the cluster were studied at the composition Pd₁₇Pt₁₇,

which were further confirmed by density functional theory (DFT) calculations. For 38-atom Pd–Pt clusters the sequence of global minima was dominated by face centered cubic (fcc) motifs based on the truncated octahedron (TO)₃₈. In the range from Pd₃₀Pt₈ to Pd₃₄Pt₄, clusters were found to be the fragment of 55-atom Mackay icosahedron. Pd₁₃Pt₂₅ cluster was an incomplete decahedron, while Pd₃₅Pt₃ was a disordered structure. For most compositions of 98-atom Pd–Pt clusters, the minima were found to have structures based on defective Marks decahedra, but in the composition range from Pd₄₆Pt₅₂ to Pd₆₃Pt₃₅, the Leary tetrahedra were the stable motifs.¹³ The onion-ring structure was determined in the Pd–Pt clusters with total 147 and 309 atoms by the same Gupta potential.¹⁴ Moreover, other bimetallic clusters such as Ag–Pd,¹³ Ag–Pt,¹⁵ Au–Pd,¹⁶ and Au–Pt¹⁷ clusters were also widely studied.

Recently, we have studied the chemical ordering and stable geometrical structures of ternary or trimetallic clusters by a global optimization algorithm, i.e., adaptive immune optimization algorithm (AIOA).¹⁸⁻²⁰ The segregation phenomena of the Cu, Ag and Au atoms in Cu–Ag–Au trimetallic clusters were investigated by the Gupta potential.²¹ Ternary Lennard-Jones clusters (TLJ) with two-body potential were investigated to study the effect of potential parameters.²² Furthermore, TLJ potential was also applied for Ar–Kr–Xe clusters, and reduced strain energies were analyzed to propose possible ways of reducing strain.²³ In 38-atom Au–Pd–Pt clusters, more structural motifs were found than bimetallic clusters containing Au, Pd or Pt atoms.²⁴ In Au₁₈Pd_nPt_{32-n} ($n = 1-31$) clusters, decahedral structures with

close packing anti-layers, twin-fcc (face-centered cubic) structures, twin-fcc with anti-layers, icosahedral (Ih) structures were found.²⁵

From the theoretical viewpoint, the DFT methods and the tight binding (TB) models were extensively used for bimetallic and trimetallic clusters.² Methods based on DFT, such as *ab initio* DFT, could be high accurate for a wide variety of systems, e.g., Ag and CdSe clusters.^{26,27} However, the process by the DFT for large systems was very time consuming. Therefore, more approximation models were developed, and the tight binding approximation might be deduced as a rigorous approximation to the DFT.²⁸ The tight binding model required a much less computational efforts than the DFT methods, although it was considered as less accurate than the DFT.

The catalytic reaction performance of trimetallic clusters are often enhanced mainly in terms of selectivity compared to bimetallic clusters, and the structures and properties of trimetallic clusters tend to be influenced by altering size and composition, which is guided to the development of trimetallic clusters. For the representing Pd–Pt clusters, the structural diversity and catalytic property might be improved by the addition of the third metallic atom. Moreover, Pd-based (Ag–Pd and Au–Pd) and Pt-based (Ag–Pt and Au–Pt) bimetallic clusters have been developed for many years in order to increase the selectivity. Therefore, the effect of Ag and Au on the stable structures of trimetallic M–Pd–Pt (M = Ag and Au) clusters was studied in this paper. To provide insight into the influence of Ag and Au dopants on the structures of M–Pd–Pt clusters, we optimized the putative global minimal structures of the studied clusters with up to 75 atoms using AIOA. The second moment

approximation to tight-binding theory (i.e., Gupta potential) was applied for describing the interaction between Ag, Au, Pd, and Pt atoms in the studied clusters. The structural and energetic differences for Ag and Au dopants in M–Pd–Pt clusters were compared.

2. Method

The interatomic interaction of trimetallic M–Pd–Pt (M = Ag and Au) clusters is described by the many-body Gupta potential, which is based on the second moment approximation to tight binding theory.²⁹ It is noted that Gupta potential has been successfully applied to study the structures of monometallic, bimetallic M–Pd and M–Pt, and trimetallic M–Pd–Pt clusters effectively.^{16,17,24,30} It has been validated to be suitable for describing M–Pd, M–Pt, and M–Pd–Pt clusters. For instance, the comparison of the Gupta potential and DFT results showed that the potential was quite accurate for intermediate compositions of 55-atom Au–Pt clusters.¹⁷ The Gupta potential (V_N) composed of repulsive pair $V^r(i)$ and attractive pair $V^m(i)$ terms can be depicted in the following form:

$$V_N = \sum_{i=1}^N \{V^r(i) - V^m(i)\} \quad (1)$$

$$V^r(i) = \sum_{j=1(j \neq i)}^n A_{ij} \exp\left(-p_{ij} \left(\frac{r_{ij}}{r_{ij}^{(0)}} - 1\right)\right) \quad (2)$$

$$V^m(i) = \left[\sum_{j=1(j \neq i)}^n \xi_{ij}^2 \exp\left(-2q_{ij} \left(\frac{r_{ij}}{r_{ij}^{(0)}} - 1\right)\right) \right]^{1/2} \quad (3)$$

where r_{ij} is the distance between atom i and j , and $r_{ij}^{(0)}$ is the equilibrium

first-neighbor distance. A_{ij} is the coefficient of the repulsive term, ξ_{ij} is an effective hopping integral between atom i and j , and p_{ij} , q_{ij} , describe their dependence on the repulsive and attractive interatomic distance, respectively. Parameters of A_{ij} , $r_{ij}^{(0)}$, p_{ij} , q_{ij} , and ξ_{ij} are derived by fitting the cohesive energy, lattice constant, and elastic constants. The corresponding parameters for the trimetallic M–Pd–Pt (M = Ag and Au) clusters used in this study are taken from Refs. [12,15,31,32], as listed in Table 1.

AIOA is adopted to locate the putative global minimal structures of trimetallic M–Pd–Pt (M = Ag and Au) clusters, which is developed based on the evolutionary ideas of natural genetic selection and clonal selection principles.¹⁹ The method has been successfully applied for the optimization of pure elemental clusters, e.g., LJ₂₀₀ clusters,¹⁹ binary or bimetallic clusters, such as Cu–Ag and Cu–Au clusters,²⁰ and ternary clusters, e.g., ternary Ar–Kr–Xe clusters,^{23,33} trimetallic Cu–Ag–Au⁵ and Au–Pd–Pt clusters.^{24,34} The basic frame of the AIOA involves the construction of original gene library, immune clone operation, and mutation operation. It starts from a population of randomly generated and local minimized individuals, which is performed by limited memory quasi-Newton algorithm (L-BFGS).³⁵ Then, in the immune clone operation, a number of individuals are selected with a probability as described in Ref. [18] to compose a gene library. Next, 50% of the individuals are randomly selected and further performed with energy-based mutation, and for the other 50% individuals two type atoms are randomly selected and their locations are exchanged, which is an atomic exchange operation.²⁰ The former operation is

applied for geometrical isomers, and the latter strategy is for homotopic problem in binary or ternary clusters. New individuals obtained by mutation operation are further compared to update the gene library, which is performed by cluster similarity checking with a connectivity table.¹⁹ At last, the repetition of the selection, mutation, and updating gene library operations is performed to locate the stable structures.

3. Results and Discussion

3.1 Geometrical structures of 13-atom M–Pd–Pt clusters

The stable structures of trimetallic $\text{Ag}_m\text{Pd}_n\text{Pt}_l$ and $\text{Au}_m\text{Pd}_n\text{Pt}_l$ ($m + n + l = 13$) clusters with all compositions are located by AIOA. Two types of minimum energy configurations can be found, i.e., Mackay icosahedron and non-icosahedron, as plotted in Figure 1a. It should be noted that the global optimization of AIOA starts from randomly generated and local minimized structures without the restriction of symmetry. Therefore, the structures as shown in Figure 1 are global minima, and only two motifs are found in 13-atom M–Pd–Pt clusters. In Figure 1a, Mackay icosahedral motif is expressed with full sphere. In the non-icosahedral motif the segment of Mackay icosahedron (9 atoms) is also drawn with full sphere, and other four atoms are shown with hollow sphere. Therefore, it can be seen that the non-icosahedron can be recognized as an incomplete Mackay icosahedron. Furthermore, optimization results indicate that the dominant structural motif of 13-atom Ag–Pd–Pt and Au–Pd–Pt clusters is the configuration with Mackay icosahedron. Non-icosahedral motifs of both clusters occur only at several

compositions, and the corresponding composition of Ag, Au, Pd and Pt is listed in Table 2. From Table 2 it can be found that 13-atom Au–Pd–Pt clusters have more non-icosahedral motifs than Ag–Pd–Pt clusters. Moreover, at some compositions, e.g., $N_{\text{Ag}} = N_{\text{Au}} = 6$, $N_{\text{Pd}} = 2$, and $N_{\text{Pt}} = 5$, both clusters have the non-icosahedral structures.

To compare the structural difference between Ag–Pd–Pt and Au–Pd–Pt clusters $\text{Ag}_3\text{Pd}_n\text{Pt}_l$ and $\text{Au}_3\text{Pd}_n\text{Pt}_l$ ($n + l = 10$) clusters shown in Figure 1b and c are taken as examples. From Figure 1b it is clear that in $\text{Ag}_3\text{Pd}_n\text{Pt}_l$ clusters, all motifs are icosahedra. In detail, for $\text{Ag}_3\text{Pd}_n\text{Pt}_l$ ($n = 1-6$) clusters, the location of three Ag atoms is same, but in $\text{Ag}_3\text{Pd}_7\text{Pt}_3$, $\text{Ag}_3\text{Pd}_8\text{Pt}_2$ and $\text{Ag}_3\text{Pd}_9\text{Pt}_1$ clusters, corresponding distribution of three Ag atoms is different from each other, and it is also different from $\text{Ag}_3\text{Pd}_n\text{Pt}_l$ ($n = 1-6$) clusters. Furthermore, in these clusters, the inner core of the Mackay icosahedra is located by Pt atoms, including on Pt atom in the inner core of $\text{Ag}_3\text{Pd}_9\text{Pt}_1$ cluster. However, for $\text{Au}_3\text{Pd}_n\text{Pt}_l$ ($n + l = 10$) clusters plotted in Figure 1c, there exist two motifs as described above. In all 13-atom icosahedral structures of $\text{Au}_3\text{Pd}_n\text{Pt}_l$ ($n = 1, 2, 6-9$) clusters, three Au atoms have the same location. The inner core of the icosahedral motif is also occupied by Pt atoms as in Ag–Pd–Pt clusters. Therefore, in small size (13-atom) M–Pd–Pt ($M = \text{Ag}$ or Au) clusters, even for the same compositions, the configurations or the atomic distribution might be different.

Figure 2 shows the local minimal and global minimal structures of $\text{Au}_3\text{Pd}_3\text{Pt}_7$ cluster. Apparently, the potential energy of the former one is only 0.026472 eV higher than that of the latter one. On the other hand, the number of bonds, that is the

number of the nearest neighbor contacts (n_{nn}), is an important property of clusters. The number n_{nn} is used here to distinguish the degree of packing, and for the clusters it is given by

$$n_{nn} = \sum_{i < j} \delta_{ij} \quad (4)$$

where $\delta_{ij} = \begin{cases} 1, & r_{ij} \leq 1.2r_{ij}^{(0)} \\ 0, & r_{ij} > 1.2r_{ij}^{(0)} \end{cases}$ $i, j = \text{Ag, Au, Pd, or Pt}$. Results show that the n_{nn} value

(i.e., 42) of local minimal clusters with Mackay icosahedral motif is significantly larger than that of global minimal structures with non-icosahedral motif (i.e., 38).

The similar difference between icosahedral and non-icosahedral motif can also be found in 13-atom Ag–Pd–Pt clusters. It can thus be concluded that in M–Pd–Pt (M = Ag or Au) clusters, the most stable structures doesn't correspond to the smallest value of bond number. This can be explained by the energies and bond number (nn) of each atom in trimetallic clusters, which is listed in Figure 2. Furthermore, in both clusters, the sequence of atomic energies from low to high is: Pt, Pd, Ag (or Au).

3.2 Geometrical structures of 34-atom M–Pd–Pt clusters

The stable structures of 34-atom $\text{Ag}_{10}\text{Pd}_n\text{Pt}_{24-n}$ and $\text{Au}_{10}\text{Pd}_n\text{Pt}_{24-n}$ ($n = 1-23$) clusters are optimized, and they are shown in Figures 3 and 4, respectively. In Figure 3, these 23 Ag–Pd–Pt clusters can be categorized into five classes, i.e., amorphous structures at $n = 1, 2, 4-6, 8,$ and 23 , decahedron at $n = 3$, five-fold structures with the inner core composed of 13-atom Mackay icosahedron at $n = 9-12, 15-17$, structures with multi 19-atom double-icosahedra at $n = 7, 13, 18-22$, and one mixed decahedral (Dh)/close-packed motif³⁰ at $n = 14$, which is a global minimal structure

found in 34-atom Pd–Pt clusters. From Figure 3 in $\text{Ag}_{10}\text{Pd}_n\text{Pt}_{24-n}$ clusters, it seems that Ag and Pd atoms tend to be on the surface, and Pt atoms prefer to locate the inner shell or core. More clearly, it is apparent that in $\text{Ag}_{10}\text{Pd}_{11}\text{Pt}_{13}$ cluster, the icosahedral inner core is occupied by all 13 Pt atoms. Furthermore, in the mixed Dh/close-packed motif of $\text{Ag}_{10}\text{Pd}_{14}\text{Pt}_{10}$, a tetrahedral core of 10 atoms are occupied by 10 Pt atoms.

In Figure 4, the motifs of $\text{Au}_{10}\text{Pd}_n\text{Pt}_{24-n}$ ($n = 1-23$) clusters can be recognized as 4 decahedra at $n = 1, 4, 8,$ and 23 , 9 partial Mackay icosahedra at $n = 2, 3, 5-7,$ $16-18,$ and 21 , 6 mixed Dh/close-packed motifs at $n = 9, 10,$ and $12-15$, and structures based on 19-atom double-icosahedra at $n = 11, 19, 20,$ and 22 . From these structures it is clear that Au and Pd atoms prefer to locate on the surface, and Pt atoms tend to be on the inner shell. In $\text{Au}_{10}\text{Pd}_{14}\text{Pt}_{10}$, the tetrahedral core of 10 atoms are occupied by Pt atoms as in $\text{Ag}_{10}\text{Pd}_{14}\text{Pt}_{10}$ cluster.

As shown in Figures 3 and 4, the atomic distribution of Pd and Pt atoms in 34-atom $\text{Ag}_{10}\text{Pd}_n\text{Pt}_{24-n}$ ($n = 1-23$) clusters is similar to that of Au–Pd–Pt clusters. However, the distribution of Ag atoms is different from that of Au atoms. Figure 5 plots the bond number of Ag–Ag and Au–Au bonds in $\text{Ag}_{10}\text{Pd}_n\text{Pt}_{24-n}$ and $\text{Au}_{10}\text{Pd}_n\text{Pt}_{24-n}$ ($n=1-23$) clusters, respectively. It can be seen that except for $n = 1$ and 4 , the bond number of Au–Au is significantly larger than that of Ag–Ag. It means that Au atoms in Au–Pd–Pt clusters grow more closely than Ag atoms in Ag–Pd–Pt clusters.

To analyze the stability of a certain composition compared to its neighbors in

trimetallic clusters, the second order finite difference $\Delta_2 E$ is applied. For example, in $\text{Ag}_{10}\text{Pd}_n\text{Pt}_{24-n}$ cluster, $\Delta_2 E$ is the energy released by migrating one Pd atom from $\text{Ag}_{10}\text{Pd}_{n+1}\text{Pt}_{23-n}$ to $\text{Ag}_{10}\text{Pd}_{n-1}\text{Pt}_{25-n}$ to form two $\text{Ag}_{10}\text{Pd}_n\text{Pt}_{24-n}$ particles. It is defined as $\Delta_2 E = E_{\min}(n+1) + E_{\min}(n-1) - 2E_{\min}(n)$ of the energy, where $E_{\min}(n)$ is the potential energy of stable structure for 34-atom $\text{Ag}_{10}\text{Pd}_n\text{Pt}_{24-n}$ and $\text{Au}_{10}\text{Pd}_n\text{Pt}_{24-n}$ clusters. Figure 6 plots $\Delta_2 E$ for $\text{Ag}_{10}\text{Pd}_n\text{Pt}_{24-n}$ and $\text{Au}_{10}\text{Pd}_n\text{Pt}_{24-n}$ ($n = 2-22$) clusters with size n . In Figure 6, the positive peaks of $\Delta_2 E$ correspond to particularly stable structures with respect to their neighbors. From the figure, three apparent positive peaks, i.e., $\text{Ag}_{10}\text{Pd}_{11}\text{Pt}_{13}$, $\text{Ag}_{10}\text{Pd}_{17}\text{Pt}_7$, and $\text{Ag}_{10}\text{Pd}_{20}\text{Pt}_4$, are found in $\text{Ag}_{10}\text{Pd}_n\text{Pt}_{24-n}$ ($n = 2-22$) clusters, and two peaks, i.e., $\text{Au}_{10}\text{Pd}_5\text{Pt}_{19}$ and $\text{Au}_{10}\text{Pd}_{14}\text{Pt}_{10}$ clusters are found in $\text{Au}_{10}\text{Pd}_n\text{Pt}_{24-n}$ clusters. This can be explained by the relatively higher point group symmetry than their neighbors (C_s), e.g., C_1 for $\text{Ag}_{10}\text{Pd}_{11}\text{Pt}_{13}$, $\text{Ag}_{10}\text{Pd}_{17}\text{Pt}_7$, $\text{Ag}_{10}\text{Pd}_{20}\text{Pt}_4$, and $\text{Au}_{10}\text{Pd}_5\text{Pt}_{19}$ and C_{2v} for $\text{Au}_{10}\text{Pd}_{14}\text{Pt}_{10}$. It can be further accounted for by low geometrical symmetry of the motifs in 34-atom M–Pd–Pt clusters as shown in Figures 3 and 4, even if the homotopic symmetry, i.e., isomers have the same geometrical arrangement but differ only for the distribution of different types of atoms, is not considered. From the curves of $\text{Ag}_{10}\text{Pd}_n\text{Pt}_{24-n}$ and $\text{Au}_{10}\text{Pd}_n\text{Pt}_{24-n}$ ($n = 2-22$) clusters, there exists no same peaks. Furthermore, these positive peaks might be designated as magic numbers observed in mass spectra.

3.3 Structural comparison between 60-atom and 75-atom M–Pd–Pt clusters

Putative stable structures of $\text{Ag}_{20}\text{Pd}_{5n}\text{Pt}_{40-5n}$ and $\text{Au}_{20}\text{Pd}_{5n}\text{Pt}_{40-5n}$ ($n = 1-7$)

clusters are shown in Figure 7. At first, $\text{Ag}_{20}\text{Pd}_5\text{Pt}_{35}$ and $\text{Ag}_{20}\text{Pd}_{10}\text{Pt}_{30}$ clusters have amorphous motifs, but the corresponding motifs of $\text{Au}_{20}\text{Pd}_5\text{Pt}_{35}$ and $\text{Au}_{20}\text{Pd}_{10}\text{Pt}_{30}$ clusters are decahedra with anti-layers. Furthermore, at $\text{Ag}_{20}\text{Pd}_{15}\text{Pt}_{25}$, cluster takes the motif of Dh/close-packed, and $\text{Au}_{20}\text{Pd}_{15}\text{Pt}_{25}$ has a decahedral motif. With the increase of size n , both $\text{Ag}_{20}\text{Pd}_{20}\text{Pt}_{20}$ and $\text{Au}_{20}\text{Pd}_{20}\text{Pt}_{20}$ clusters have the Dh/close-packed motifs. Apparently, in these Dh/close-packed motifs, the inner decahedral core of 22-atom is almost occupied by Pt atoms. Next, $\text{Ag}_{20}\text{Pd}_{25}\text{Pt}_{15}$ cluster has a ring-like structure linked by three face-sharing double icosahedra as in Cu-Ag-Au clusters.²¹ Furthermore, $\text{Ag}_{20}\text{Pd}_{30}\text{Pt}_{10}$ cluster is recognized as a type of square crossing for two pancake structures, and all Pt atoms are laid in the inner shell. At $\text{Ag}_{20}\text{Pd}_{35}\text{Pt}_5$ cluster, the growth is based on a complete 55-atom Mackay icosahedron. On the other hand, $\text{Au}_{20}\text{Pd}_{5n}\text{Pt}_{40-5n}$ ($n = 5-7$) clusters take the same icosahedral motifs as in $\text{Ag}_{20}\text{Pd}_{35}\text{Pt}_5$.

Figure 8 plots the stable structures of $\text{Ag}_{25}\text{Pd}_{5n}\text{Pt}_{50-5n}$ and $\text{Au}_{25}\text{Pd}_{5n}\text{Pt}_{50-5n}$ ($n = 1-9$) clusters. From Figure 8a it can be found that the dominant motif in 75-atom Ag-Pd-Pt clusters is Dh/close-packed, except for amorphous structure at $n = 1$ and the segment of complete 147-atom Mackay icosahedron at $n = 8$. However, from Figure 8b it can be seen that the dominant motif of 75-atom Au-Pd-Pt clusters is complete 75-atom Marks decahedron. For $\text{Au}_{25}\text{Pd}_{5n}\text{Pt}_{50-5n}$ ($n = 4, 5, \text{ and } 7$) clusters, the structures take the form of Dh/close-packed. Moreover, the inner core of $\text{Au}_{25}\text{Pd}_{25}\text{Pt}_{25}$ is 39-atom Ino-decahedron. Moreover, the distribution of Ag, Au, Pd, and Pt in large 60- and 75-atom clusters is consistent with that of 34-atom clusters,

which can be explained by surface energy.³⁴

4. Conclusions

The putative stable structures of M–Pd–Pt (M = Ag and Au) clusters with 13, 34, 60, and 75 atoms are investigated by using global optimization algorithm (i.e., adaptive immune optimization algorithm). Mackay icosahedral and non-icosahedral motifs were found in 13-atom Ag–Pd–Pt and Au–Pd–Pt clusters. For large size clusters results show that the atomic distribution of Pd and Pt atoms in the former is similar to that of the latter one. However, Au atoms in the latter one grow more closely than Ag atoms in the former one. For $M_{10}Pd_nPt_{24-n}$ ($n = 1-23$) clusters, Ag–Pd–Pt clusters can be categorized into five classes, and four classes are found in Au–Pd–Pt clusters. In 75-atom Ag–Pd–Pt clusters, the dominant motif is decahedron/close-packed motif, and in Au–Pd–Pt clusters corresponding motif is Marks decahedron.

Acknowledgements

This study is supported by National Natural Science Foundation of China (NNSFC) (Grant Nos. 21203002 and 21171008) and Anhui Provincial Natural Science Foundation (No. 1308085QB29).

References

1. B. Paramanik and A. Patra, *J. Mater. Chem. C*, 2014, **2**, 3005.

2. R. Ferrando, J. Jellinek and R. L. Johnston, *Chem. Rev.*, 2008, **108**, 845.
3. B. K. Teo, H. Zhang, X. B. Shi, *J. Am. Chem. Soc.*, 1993, **115**, 8489.
4. J. H. Sinfelt, *Acc. Chem. Res.*, 1997, **10**, 15.
5. C. N. R. Rao, G. U. Kulkarni, P. J. Thomas and P. P. Edwards, *Chem. Soc. Rev.*, 2000, **29**, 27.
6. A. Olivas, J. Antúnez-García, S. Fuentes, D. H. Galván, *Cata. Today*, 2014, **220-222**, 106.
7. H. J. Zhang, M. Okumura and N. Toshima, *J. Phys. Chem. C*, 2011, **115**, 14883.
8. X. Zhang, F. Zhang and K. Y. Chan, *Catal. Comm.*, 2004, **5**, 749.
9. W. Chanmanee, N. R. Tacconi, K. Rajeshwar, W. Y. Lin, L. Nikiel and W. A. Wampler, *J. Electrochem. Soc.*, 2012, **159**, 226.
10. Z. Zhao, M. J. Li, D. J. Cheng and J. Q. Zhu, *Chem. Phys.*, 2014, **441**, 152.
11. B. Pawelec, R. Mariscal, R. M. Navarro, S. V. Bokhorst, S. Rojas and J. L. G. Fierro, *Appl. Catal. A*, 2002, **225**, 223.
12. G. Rossi, R. Ferrando, A. Rapallo, A. Fortunelli, B. C. Curley, L. D. Lloyd and R. L. Johnston, *J. Chem. Phys.*, 2005, **122**, 194309.
13. L. O. Paz-Borbón, T. V. Mortimer-Jones, R. L. Johnston, A. Posada-Amarillas, G. Barcaro and A. Fortunelli, *Phys. Chem. Chem. Phys.*, 2007, **9**, 5202.
14. D. J. Cheng, W. C. Wang and S. P. Huang, *J. Phys. Chem. B*, 2006, **110**, 16193.
15. A. Logsdail, L. O. Paz-Borbón and R. L. Johnston, *J. Comput. Theo. Nanosci.*, 2009, **6**, 857.
16. F. Pittaway, L. O. Paz-Borbón, R. L. Johnston, H. Arslan, R. Ferrando, C.

- Mottet, G. Barcaro and A. Fortunelli, *J. Phys. Chem. C*, 2009, **113**, 9141.
17. D. Bochicchio, F. Negro and R. Ferrando, *Comput. Theor. Chem.*, 2013, **1021**, 177.
18. X. G. Shao, L. J. Cheng and W. S. Cai, *J. Chem. Phys.*, 2004, **120**, 11401.
19. L. J. Cheng, W. S. Cai and X. G. Shao, *Chem. Phys. Lett.*, 2004, **389**, 309.
20. X. Wu, W. S. Cai and X. G. Shao, *J. Comput. Chem.*, 2009, **30**, 1992.
21. X. Wu, G. H. Wu, Y. C. Chen and Y. Y. Qiao, *J. Phys. Chem. A*, 2011, **115**, 13316.
22. X. Wu, Y. Sun, C. S. Li and W. Yang, *J. Phys. Chem. A*, 2012, **116**, 8218.
23. X. Wu, Y. Sun, Y. C. Gao and G. H. Wu, *J. Mol. Model.*, 2013, **19**, 3119.
24. G. H. Wu, Q. M. Liu and X. Wu, *Chem. Phys. Lett.*, 2015, **672**, 92.
25. X. Wu and Y. J. Dong, *New J. Chem.*, 2014, **38**, 4893.
26. M. L. Tiago, J. C. Idrobo, S. Ögüt, J. Jellinek, and J. R. Chelikowsky, *Phys. Rev. B*, 2009, **79**, 155419.
27. P. Karamanis, G. Maroulis and C. Pouchan, *J. Chem. Phys.*, 2006, **124**, 071101.
28. W. M. C. Foulkes, *Phys. Rev. B*, 1993, **48**, 14216.
29. R. P. Gupta, *Phys. Rev. B*, 1981, **23**, 6265.
30. L. O. Paz-Borbón, R. L. Johnston, G. Barcaro and A. Fortunelli, *J. Phys. Chem. C*, 2007, **111**, 2936.
31. C. Massen, T. V. Mortimer-Jones and R. L. Johnston, *J. Chem. Soc. Dalton Trans.*, 2012, **23**, 4375.
32. L. O. Paz-Borbón, R. L. Johnston, G. Barcaro and A. Fortunelli, *J. Chem. Phys.*,

2008, **128**, 134517.

33. X. Wu, C. F. Huang, Y. Sun and G. H. Wu, *Chem. Phys.*, 2013, **425**, 69.
34. X. Wu and Y. J. Dong, *New J. Chem.*, 2014, **38**, 4893.
35. D. C. Liu and J. Nocedal, *Math. Program*, 1989, **45**, 503.

Table 1. Gupta potential parameters for trimetallic Ag–Pd–Pt and Au–Pd–Pt clusters.

Compositions	A_{ij} (eV)	ξ_{ij} (eV)	p_{ij}	q_{ij}	$r_{ij}^{(0)}$ (Å)
Ag–Ag	0.1031	1.1895	10.85	3.18	2.8921
Au–Au	0.2016	1.79	10.229	4.036	2.8840
Pd–Pd	0.1746	1.718	10.867	3.742	2.7485
Pt–Pt	0.2975	2.695	10.612	4.004	2.7747
Ag–Pd	0.161	1.5597	10.895	3.492	2.82
Au–Pd	0.19	1.75	10.54	3.89	2.816
Ag–Pt	0.175	1.79	10.73	3.57	2.833
Au–Pt	0.250	2.20	10.42	4.02	2.830
Pd–Pt	0.23	2.2	10.74	3.87	2.76

Table 2. Composition of 13-atom Ag–Pd–Pt and Au–Pd–Pt clusters with non-icosahedral motifs.

Ag-Pd-Pt clusters			Au-Pd-Pt clusters					
N_{Ag}	N_{Pd}	N_{Pt}	N_{Au}	N_{Pd}	N_{Pt}	N_{Au}	N_{Pd}	N_{Pt}
1	7	5	1	5	7	3	5	5
4	5	4	1	6	6	4	3	6
5	3	5	1	7	5	4	4	5
5	4	4	1	8	4	5	2	6
6	1	6	2	4	7	5	3	5
6	2	5	2	5	6	6	1	6
6	3	4	2	6	5	6	2	5
7	1	5	2	7	4	7	1	5
7	2	4	3	3	7			
8	1	4	3	4	6			

Figure Captions

- Fig. 1 a) Icosahedral and non-icosahedral motifs in $\text{Ag}_m\text{Pd}_n\text{Pt}_l$ and $\text{Au}_m\text{Pd}_n\text{Pt}_l$ ($m + n + l = 13$) clusters, and stable structures of b) $\text{Ag}_3\text{Pd}_n\text{Pt}_l$ and c) $\text{Au}_3\text{Pd}_n\text{Pt}_l$ ($n + l = 10$) clusters.
- Fig. 2. Comparison of bond numbers and atomic energies between local minimum and global minimum structures of $\text{Au}_3\text{Pd}_3\text{Pt}_7$ cluster.
- Fig. 3. Putative global minimal structures of $\text{Ag}_{10}\text{Pd}_n\text{Pt}_{24-n}$ ($n = 1-23$) clusters, and Ag, Pd, and Pt atoms are represented by red, green, and blue spheres, respectively.
- Fig. 4. Putative global minimal structures of $\text{Au}_{10}\text{Pd}_n\text{Pt}_{24-n}$ ($n = 1-23$) clusters, and Au, Pd, and Pt atoms are represented by yellow, green, and blue spheres, respectively.
- Fig. 5. Number of Ag–Ag and Au–Au bonds in $\text{Ag}_{10}\text{Pd}_n\text{Pt}_{24-n}$ and $\text{Au}_{10}\text{Pd}_n\text{Pt}_{24-n}$ ($n = 1-23$) clusters.
- Fig. 6. Second finite differences of the energies (Δ_2E) of the optimized $\text{Ag}_{10}\text{Pd}_n\text{Pt}_{24-n}$ and $\text{Au}_{10}\text{Pd}_n\text{Pt}_{24-n}$ ($n = 1-23$) clusters.
- Fig. 7. Putative global minimal structures of $\text{Ag}_{20}\text{Pd}_{5n}\text{Pt}_{40-5n}$ and $\text{Au}_{20}\text{Pd}_{5n}\text{Pt}_{40-5n}$ ($n = 1-7$) clusters, and Ag, Au, Pd, and Pt atoms are represented by red, yellow, green, and blue spheres, respectively.
- Fig. 8. Putative global minimal structures of a) $\text{Ag}_{25}\text{Pd}_{5n}\text{Pt}_{50-5n}$ and b) $\text{Au}_{25}\text{Pd}_{5n}\text{Pt}_{50-5n}$ ($n = 1-9$) clusters, and Ag, Au, Pd, and Pt atoms are represented by red, yellow, green, and blue spheres, respectively.

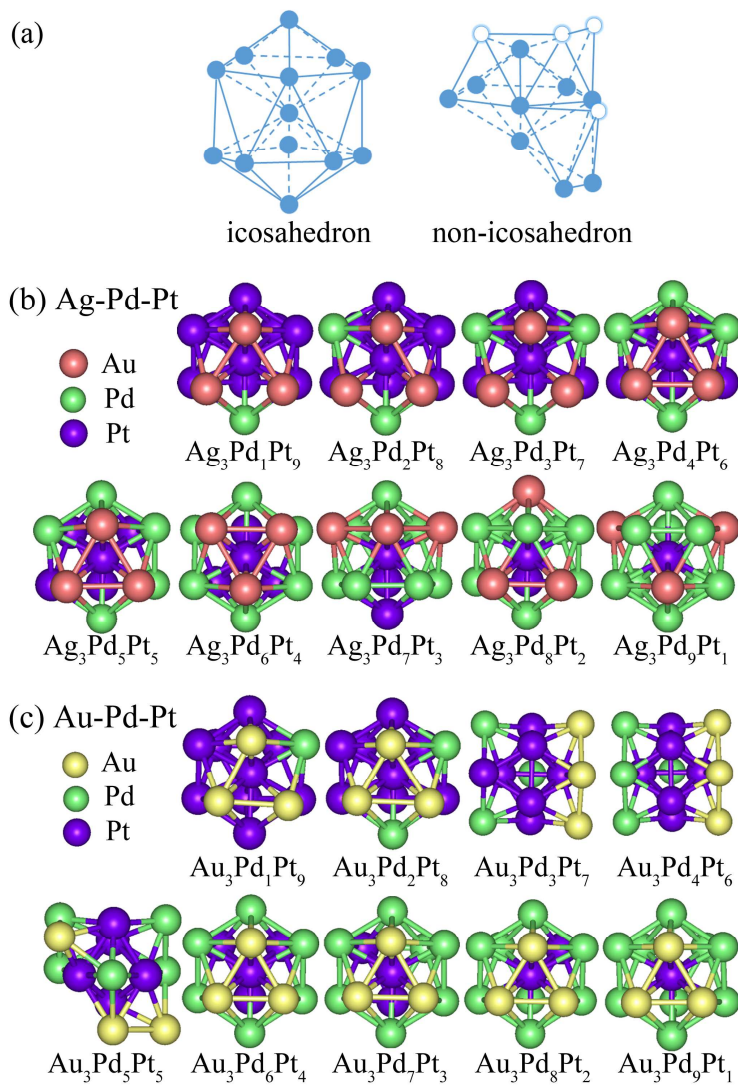


Figure 1

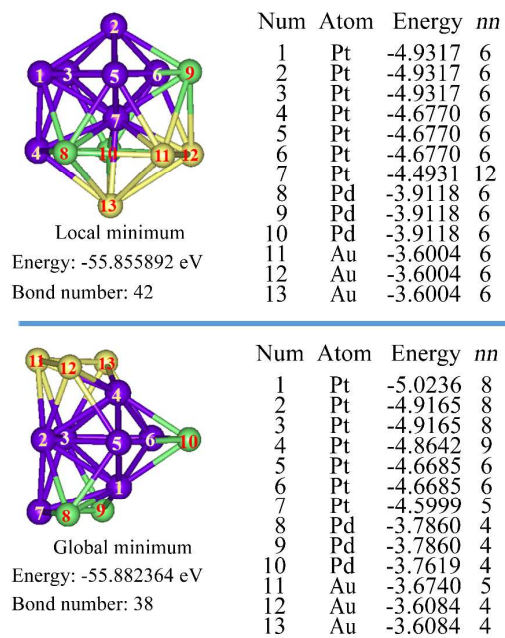


Figure 2

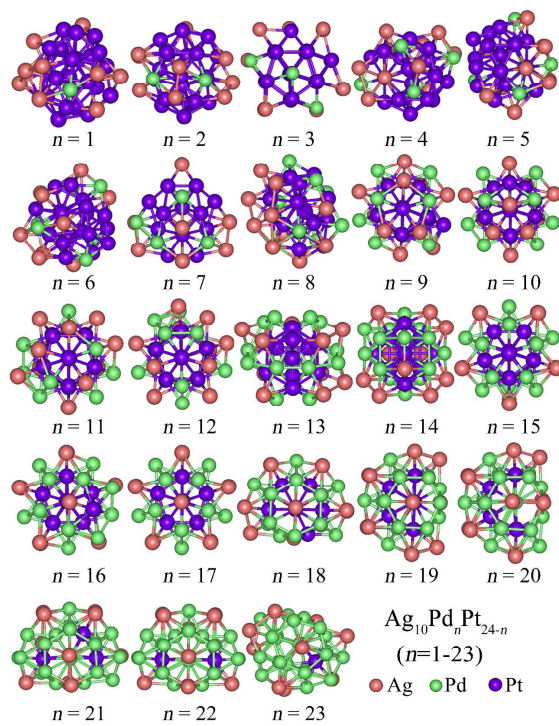


Figure 3

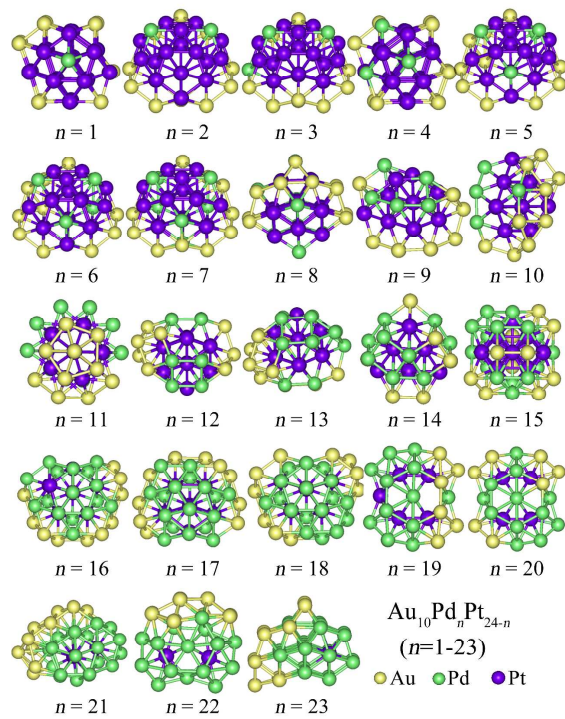


Figure 4

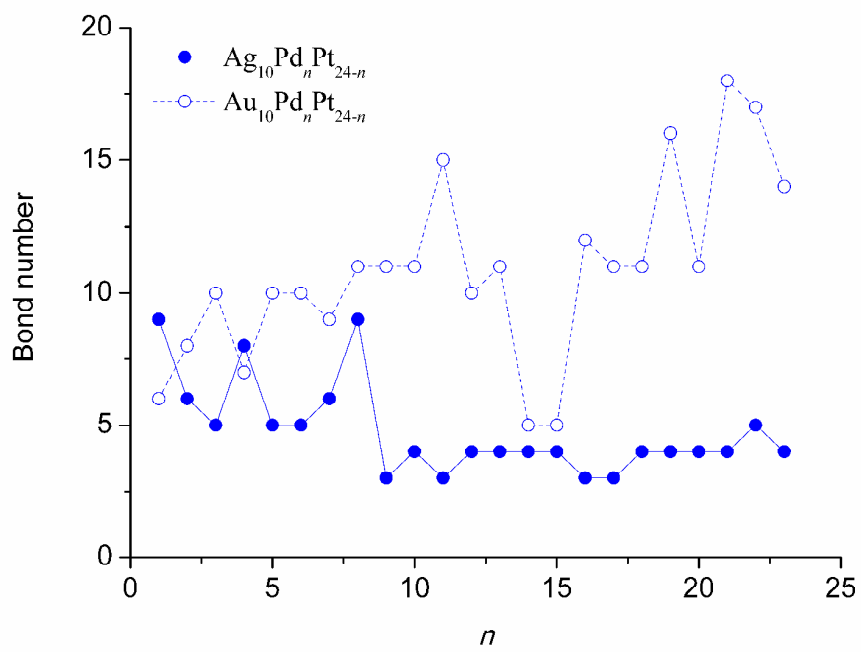


Figure 5

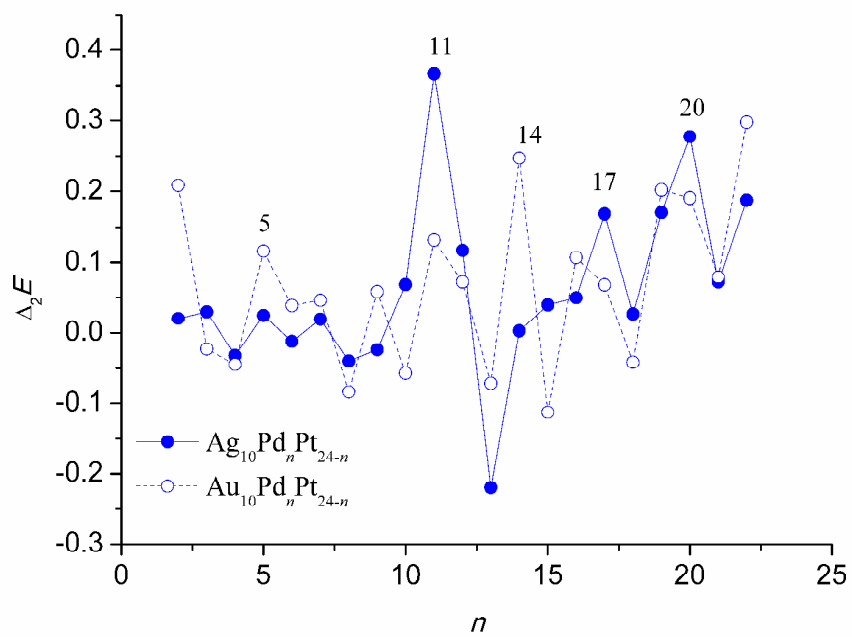


Figure 6

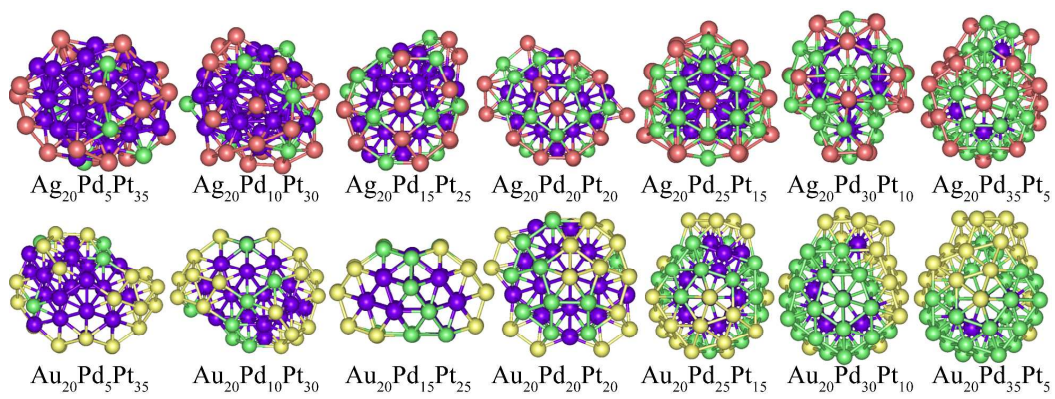


Figure 7

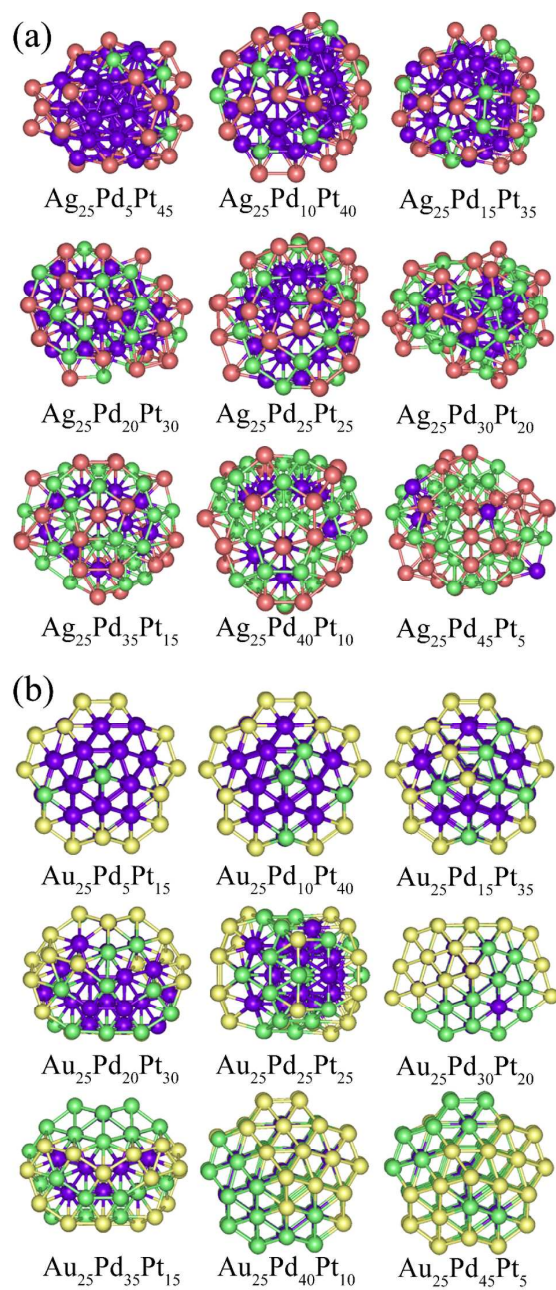


Figure 8

Highlights:

> The structures of M–Pd–Pt (M = Ag and Au) clusters are significantly affected by Ag and Au dopants.